

# Probing Laser-Induced Plasma Generation in Liquid Water

Jiyu Xu, Daqiang Chen, and Sheng Meng\*



Cite This: *J. Am. Chem. Soc.* 2021, 143, 10382–10388



Read Online

ACCESS |



Metrics & More

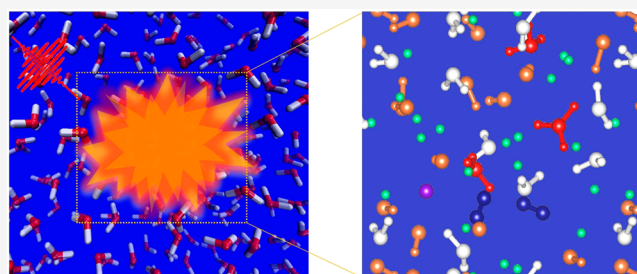


Article Recommendations



Supporting Information

**ABSTRACT:** Understanding photoexcitation dynamics in liquid water is of crucial significance for both fundamental scientific exploration and technological applications. Despite the observations of photoinduced macroscopic phenomena, the initial atomistic movements and associated energy transfer pathways immediately following laser irradiation are hard to track due to the extreme complexity of laser–water interaction and its ultrafast time scale. We explore the femtosecond evolution of liquid water upon intense photoexcitation based on nonadiabatic quantum dynamics simulations. Separate ionic and electronic dynamics were explicitly monitored with tremendous details unveiled on an unprecedented



microscopic level. Water was found to undergo the two-step heating processes. The strong-field effects and electronic excitations dominate the first-stage heating and pressurization. Subsequent relaxation of ionic and electronic subsystems further increases the ionic temperature but releases the large internal pressure. The water molecules are stretched during the laser pulses, and the electronic excitations result in the proton transfers after laser pulses. Intense laser pulses violently excite liquid water, giving rise to severe molecular dissociation and plasma generation during the laser pulses. The laser-induced water plasma is characterized by a high fraction of free protons (~50%), nonequilibrium ionic and electronic distributions, and a metallic electronic density of states.

## INTRODUCTION

The photoinduced dynamics of water is of fundamental significance to chemistry,<sup>1</sup> energy science,<sup>2,3</sup> atmospheric science,<sup>4</sup> and biology.<sup>5</sup> The common products of photoexcitation, hydrated electrons<sup>6–8</sup> and cationic holes ( $\text{H}_2\text{O}^+$ ),<sup>9</sup> have been extensively studied. The elemental processes of water upon photoexcitation and photoionization span several orders of characteristic time scales.<sup>5,10–13</sup> The intriguing macroscopic phenomena, such as plasma generation,<sup>14,15</sup> shock-wave emission,<sup>16</sup> spallation,<sup>17</sup> and drastic explosion,<sup>18</sup> can be induced via violent irradiation of water and recorded with high-speed imaging technologies. However, the microscopic dynamics of photoexcited liquid water commonly escape direct experimental measurements, and the detection of initial atomistic dynamics has to resort to ultrafast probe techniques. Recently, the ultrafast formation of OH and the dynamics of valence hole were tracked with the tunable femtosecond X-ray pulses.<sup>9</sup> The strong femtosecond X-ray pulses were also found to induce severe ionization and nonthermal heating of water, before water transforms into a disordered plasma state.<sup>14</sup> Similarly, the intense 800 and 532 nm pulses could ionize liquid water via strong-field ionization processes.<sup>15,19,20</sup> In turn, the ultrafast nuclei motions were found to mediate electron autoionization and charge separation processes.<sup>21</sup> The atomistic processes and energy transfer pathways immediately following photoexcitation are intricate but hard to track due to their ultrafast time scales.

The investigation of photoinduced dynamics would greatly benefit from theoretical explorations, but to date the latter are rather limited to a few feasible approaches. Adiabatic *ab initio* molecular dynamics simulations have provided insights into some separate processes, for example, the ultrafast dynamics of the cationic hole<sup>22</sup> and the energy absorption of terahertz pulses.<sup>23</sup> Classical molecular dynamics simulations are used to perform large-scale and long-time simulations, but the accuracy is strongly dependent on the construction of the nonadiabatic potential energy surfaces.<sup>24–26</sup> The accurate and complete descriptions require the real-time nonadiabatic *ab initio* molecular dynamics simulations. However, these simulations are commonly limited to a time scale of tens of femtosecond (fs) due to requirements of high accuracy and unprecedented computational costs for dynamic evolutions.<sup>27–29</sup> Therefore, modeling of finite-sized nanoclusters is the common practice in previous studies. For example, the photolysis of water molecules was observed in photoexcited water dimers,<sup>30,31</sup> and the processes following singlet photoexcitation and vertical photoionization were investigated in a 27-water-molecule nanocluster.<sup>32,33</sup> The long-time, fully *ab initio*, nonadiabatic

Received: May 5, 2021

Published: July 1, 2021



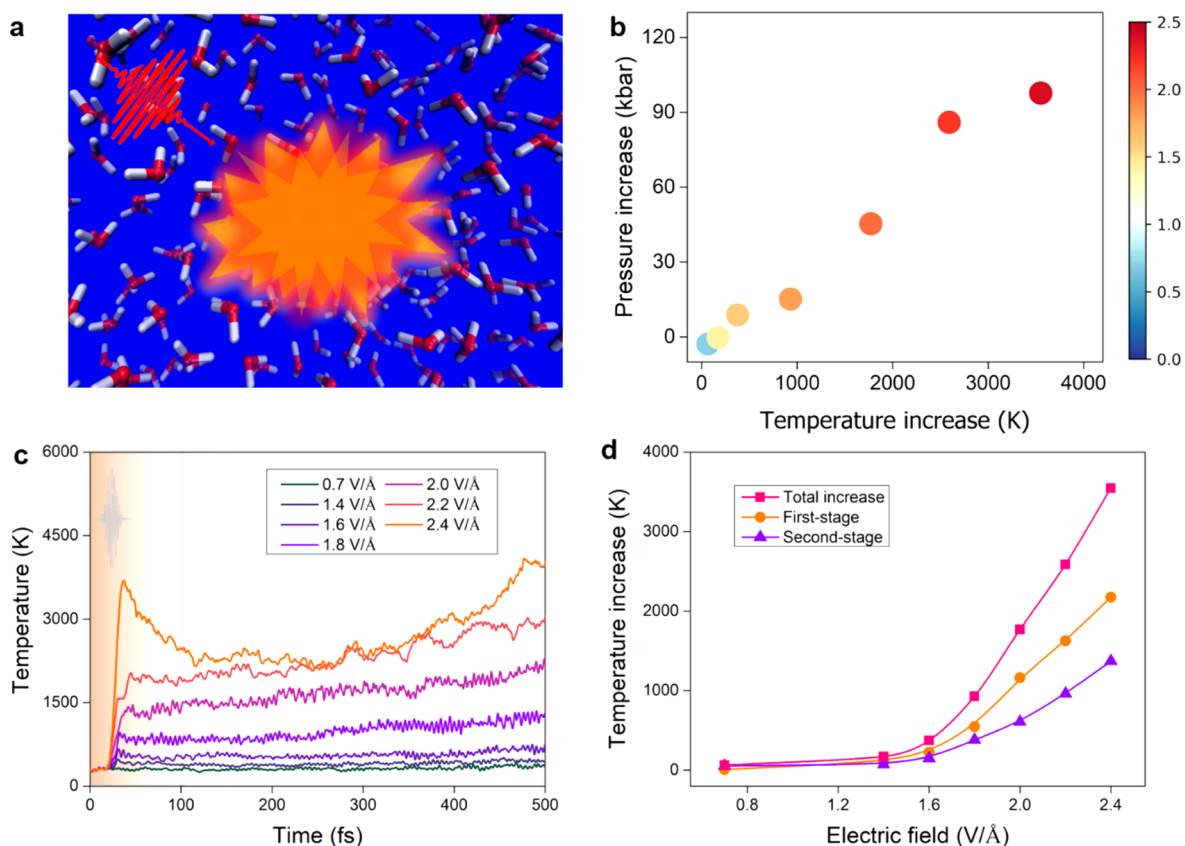


**Figure 1.** Photoinduced dynamics of liquid water. (a) Schematic diagram shows the liquid water irradiated with the 800 nm laser pulses. (b) Increase of ionic temperature versus the increase of system pressure. The colorbar shows the electric field of the pulses, and the units are V/Å. (c) Temporal evolutions of ionic temperatures with the electric field of laser pulses. The light envelope is shown in the inset. The vertical line marks the separation of the first and second stage. (d) Two-step ionic heating of liquid water.

molecular dynamics simulations of photoexcited liquid water are highly desirable but were scarcely done until now.

In this work, we employ newly developed real-time time-dependent density functional theory (rt-TDDFT) methods to simulate photoinduced dynamics of liquid water. The picosecond long nonadiabatic simulations reveal separate ionic and electronic dynamic characteristics of photoexcited liquid water. Water undergoes the two-step heating and pressurization processes upon photoexcitation. The strong-field effects of laser pulses and the electron excitations dominate the first-stage heating and the pressurization. The second-stage evolutions are subjected to the relaxation of ionic and electronic subsystems. The laser pulses greatly stretch water molecules during the laser pulses, and the electronic excitations lead to proton transfers after laser pulses. The liquid water can be severely excited with the intense laser pulse, and the violent electron excitation and water dissociation give rise to the generation of nonequilibrium and metallic water plasma.

## RESULTS AND DISCUSSION

**Two-Step Heating and Pressurization.** After equilibrium, the liquid water was isochorically irradiated with the laser pulse of  $E(t) = E_0 \cos[2\pi(c/\lambda)t] \exp[-(t - t_0)^2/2\sigma^2]$  (Figure 1a). We chose the ultrafast laser pulses with the wavelength  $\lambda = 800$  nm and the width  $\sigma = 5$  fs centered at  $t_0 = 24$  fs. The maximum electric field  $E_0$  ranges from 0.7 to 2.4 V/Å, and the corresponding peak intensities are on the order of  $10^{13}$  W/cm<sup>2</sup>. All nonadiabatic *ab initio* molecular dynamics simulations were performed for 500 fs. With the irradiations of

laser pulses, liquid water is excited undergoing successive nonequilibrium evolutions within both the ionic and electronic subsystem. To facilitate our analysis, we averaged the configurations from 450 to 500 fs as the final states of nonadiabatic simulations. Liquid water is weakly affected by weak laser pulses, while it is severely heated and pressurized with strong laser pulses (Figure 1b). With a strong laser pulse of  $E_0 = 2.4$  V/Å, the ionic subsystem of liquid water can be heated by  $\sim 3500$  K, and the system pressure is increased by  $\sim 100$  kbar in 500 fs. The increase of ionic temperature is proportional to the increase of system pressure. The rapid heating and pressurization may lead to macroscopic phenomena such as shock wave emission, cavitation, and explosion.<sup>11,15,17</sup>

Figure 1c reveals that the ionic subsystems exhibit the two-step heating processes for all the laser pulses. The first-stage heating is coincident with the envelope of the laser pulses ( $t < 50$  fs), while the second-stage heating occurs during the relaxations of the photoexcited liquid water. For convenience, we averaged the configurations from 75 to 125 fs to define the intermediate states. Figure 1d shows that the contributions of first stage to the overall temperature increase are larger than those of the second stage within the 500 fs long simulations, both of which are nonlinear with the electric field of laser pulses. The similar heating effects during laser pulses are observed with the terahertz irradiations.<sup>23</sup> The evolution of system pressure also exhibits the two-step processes despite the intrinsic large fluctuations (Figure S1a). The first stage dominates the increase of pressure, which exhibits the

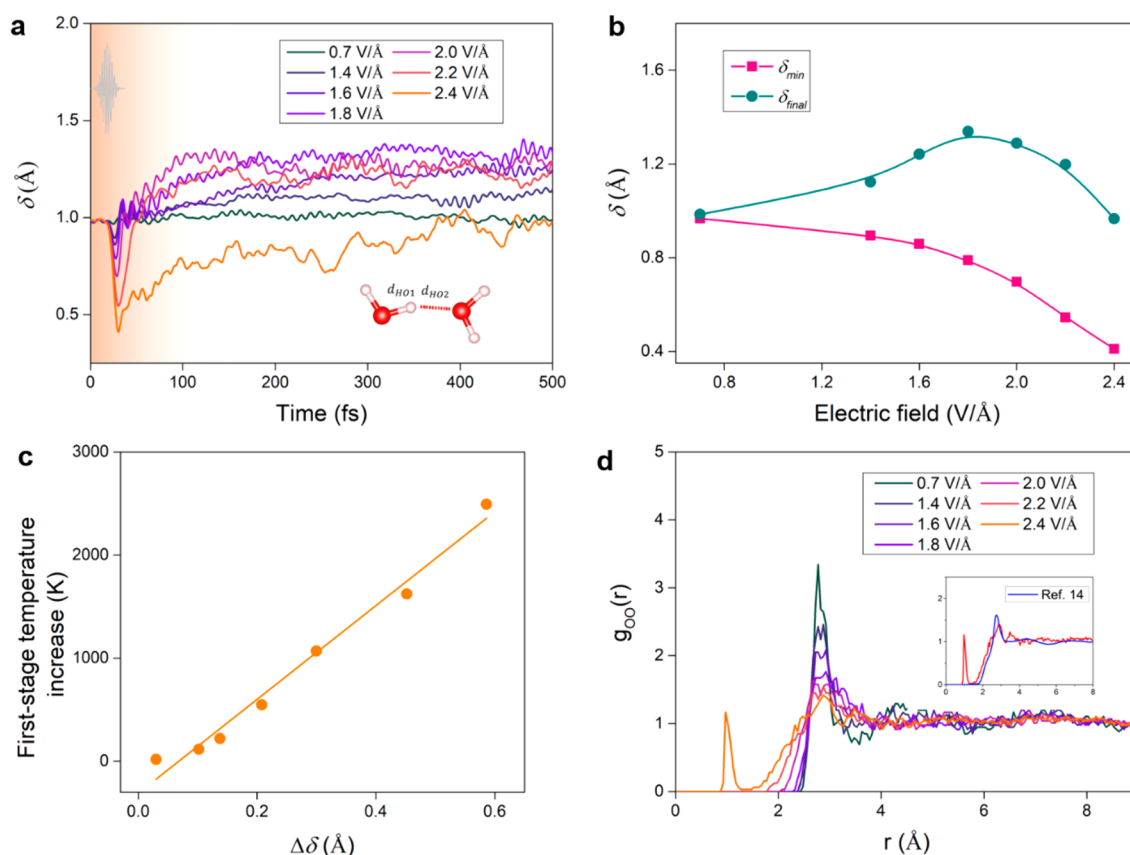


**Figure 2.** Ionic dynamics of liquid water. (a) Temporal evolutions of average  $\delta$  of all hydrogen atoms with electric field. The definition of  $\delta$  is shown in the inset. (b) Minimum of average  $\delta$  and the final  $\delta$  with electric fields of laser pulses. (c) Decrease of average  $\delta$  vs the first-stage ionic temperature increase. (d) Oxygen–oxygen radial distribution functions with the electric field of laser pulses. The radial distribution functions are calculated with the whole 500 fs long simulations for each electric field. The inset shows the comparison with the data from ref 14.

nonlinear relationship with the electric field of laser pulses. On the other hand, the relaxation processes lead to the slight decrease of pressure in the second stage (Figure S1b). These nonlinear relationships reflect that a great amount of energy can be absorbed under strong laser pulses (Figure S2).

**Ionic Dynamics.** To reveal the underlying mechanisms, we tracked the ionic dynamics of liquid water. The proton transfer coordinate is defined as the distance difference between each hydrogen atom (H) and its two nearest oxygen atoms (O1 and O2),  $\delta = |d_{\text{HO1}} - d_{\text{HO2}}|$ . Figure 2a shows the evolutions of the average  $\delta$  of all hydrogen atoms in the simulations. Initially,  $\delta$  is  $\sim 1$  Å, corresponding to the undisturbed hydrogen-bond (H-bond) network of liquid water. With the weak pulse of  $E_0 = 0.7$  V/Å, the average  $\delta$  hardly changes, and the H-bond network remains unaffected. With stronger laser pulses of  $E_0 > 1.4$  V/Å, the average  $\delta$  undergoes the sudden decrease during the laser illumination, and the minimum  $\delta_{\text{min}}$  exhibits a nonlinearity with the electric field and even reaches  $\sim 0.4$  Å with intense laser pulses (Figure 2b). The decrease of  $\delta$  reflects the stretch and break of OH bonds during laser irradiation (Figure S3) and can be used to denote energy transferred to the nuclei and the heating effects in the first stage. The nice linear relationship is obtained in Figure 2c. As these events occur during laser irradiation, field effects dominate the ionic dynamics at this stage.<sup>34</sup>

After laser illumination, the photoexcited liquid water undergoes a fast equilibration of  $\sim 100$  fs to relax the stretched H-bond network. The stretched water molecules can return to the normal molecular configuration, leading to recovery of

average  $\delta$  in Figure 2a. The detailed analysis reveals that some protons shuttle between its two nearest oxygen atoms under laser electric fields  $E_0 \geq 1.8$  V/Å (Figure S3). The proton transfer is attributed to the excitations of electrons and the softening of OH bonds in water, and the shuttling is due to the competition of neighboring excited water molecules and the heated states. The average times of first-time proton transfer ( $t - t_0$ ) are 72 and 65 fs with the electric field of 1.8 and 2.0 V/Å, respectively (Figure S3 and Table S1). Similar proton transfer and OH formation were also observed in photoionized liquid water, occurring with a time scale of  $\sim 46$  fs.<sup>9</sup> The protons may not bond back to the original oxygen atoms when the laser electric field is  $> 2.0$  V/Å, leading to the ultimate dissociation of water molecules.

At last, the  $\delta_{\text{final}}$  is reached after the slow equilibration process of  $\sim 300$  fs, shown in Figure 2b. The  $\delta_{\text{final}}$  increases with electric field under medium-strength laser pulses ( $1.4$  V/Å  $\leq E_0 \leq 1.8$  V/Å), indicating that the heating effects of laser pulses only distort the H-bond network of liquid water (Figure S4a). The average H-bond angle is increased by  $\sim 20^\circ$  with the electric field  $E_0 = 1.8$  V/Å. Each water molecule still exhibits the normal bond length and bond angle even with the electric field  $E_0 = 2.0$  V/Å (Figure 3a and Figure S4b). However, the  $\delta_{\text{final}}$  begins to decrease with  $E_0 = 2.0$  V/Å, which is due to the decrease of oxygen–oxygen distance in Figure 2d and the water dissociations. Even, the severe dissociation of water molecules gives rise to the formation of free protons amounting to a portion of  $\sim 50\%$  under the laser electric field of  $2.4$  V/Å (Figure S5), leading to  $\delta < 1$  in the whole 500 fs simulation.

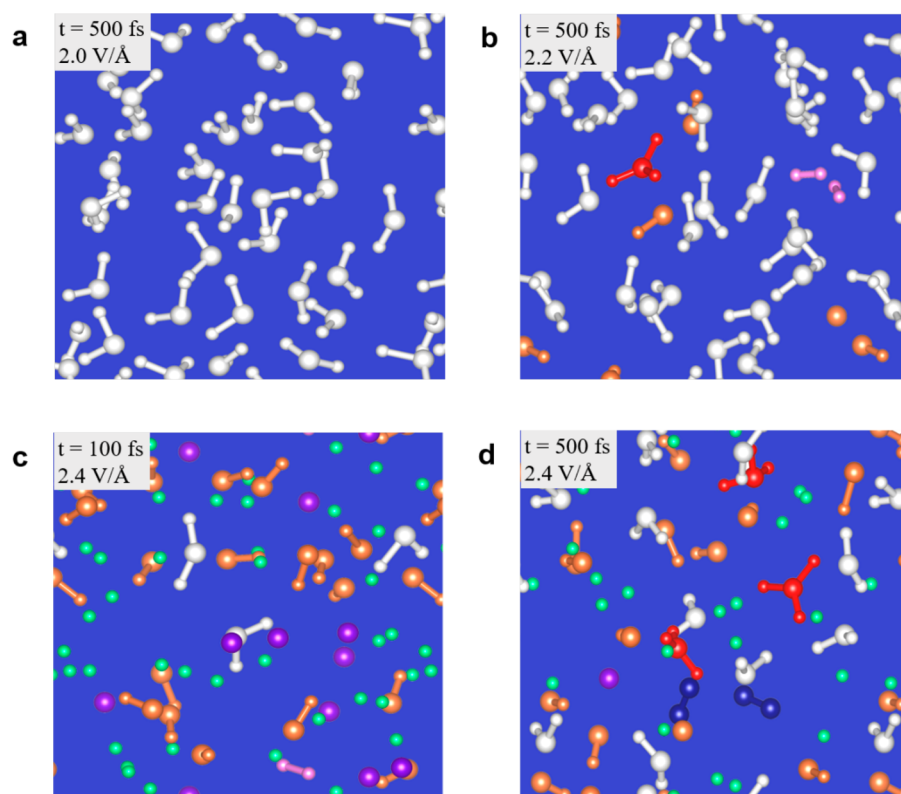


**Figure 3.** (a–d) Configurations of the nonadiabatic *ab initio* molecular dynamics simulations. The electric field of laser pulses and the time are shown in the inset. The water molecules, hydroniums, hydroxyls, free protons and oxygens, transient hydrogen molecules, and oxygen molecules are shown in white, red, orange, green, purple, pink, and dark blue colors, respectively.

Both the heating effects and water dissociations contribute to the disordering of water, which is demonstrated in the distributions of radial distribution functions (RDFs) (Figure 2d and Figure S6). The conventional first peak at  $r \sim 2.8 \text{ \AA}$  in oxygen–oxygen RDF is broadened under the electric field of laser pulses, and the conventional second peak at  $r \sim 4.5 \text{ \AA}$  is even smoothed away. Interestingly, the oxygen–oxygen and hydrogen–hydrogen RDFs show the formation of transient oxygen and hydrogen molecules with the laser pulses of  $E_0 = 2.2\text{--}2.4 \text{ V/\AA}$ , consistent with the experimental measurements.<sup>35</sup> The detailed analysis shows that the violent water dissociation gives rise to the generation of various intermediate species in liquid water. The free protons and oxygens, hydroniums, hydroxyls, transient hydrogen molecules, and oxygen molecules are shown in Figure 3b–d, and the formation of these species relies on the capture of initially generated free protons (Figure 3c,d and Figure S5).

**Electronic Dynamics.** The evolution of ionic subsystems is strongly related to time-dependent electron occupation of electronic subsystems, which determines the nonadiabatic potential energy surfaces. As shown in Figure 4a, the 800 nm laser pulses excite the valence electrons, and the excited electrons are relaxed via the subsequent electron–electron and electron–ion interactions. We defined the effective electron excitations by the number ratio of valence electrons excited at  $t = 100 \text{ fs}$ . The effective electron excitations exhibit a nonlinear relationship with electric field in Figure 4b. The nonlinearity reflects the transition from multiphoton to strong-field ionization processes, and the threshold of  $E_0 = \sim 1.9 \text{ V/\AA}$  is consistent with the estimation of  $1.0\text{--}2.0 \text{ V/\AA}$  for laser wavelength  $\lambda = 800 \text{ nm}$  with Keldysh’s method.<sup>5,36,37</sup> The

fraction of excited valence electrons reaches  $\sim 12\%$  with the laser electric field of  $2.4 \text{ V/\AA}$ . The electron excitations greatly enhance the internal pressure of liquid water and dominate the pressure increase in the first stage (Figure S1c). At the same time, the electron excitations facilitate the aforementioned proton transfer and water dissociation during the fast equilibrium processes.<sup>9</sup> As shown in Figure S7, the electronic occupation of excited liquid water exhibits the quasi-Fermi–Dirac distributions, and the electronic subsystems are heated to over 10000 K. The number of excited electrons decrease with time, leading to the cooling of electronic subsystems.<sup>38</sup> The number of electronic recombination increases with the initial electronic excitations (Figure 4b), and the time constant of recombination is  $\sim 0.3 \text{ ps}$  (Figure S8). We note that the finite-size effects of theoretical simulations may overestimate the recombination rate, and the excited electrons can be ejected away, leading to the increase of electron–hole separation ( $>10 \text{ \AA}$ ) in experiments.<sup>9,39,40</sup>

The energy transfer between electronic and ionic subsystems relies on the concurrent electron–phonon coupling processes, and the energy transfer leads to the second-stage heating and the structural distortion of ionic subsystems during the slow equilibrium processes. The linear relationship is also obtained between the electron recombination and the second-stage temperature increases (Figure 4c). The decrease of electron excitations releases the internal pressure, and this effect exceeds that of ionic kinetic increases (Figure S1d). Thus, the relaxation processes of electronic and ionic subsystems give rise to the decrease of pressure in the second stage. In essence, these nonlinearities of ionic temperatures and system pressures with electric fields can be attributed to the transition from

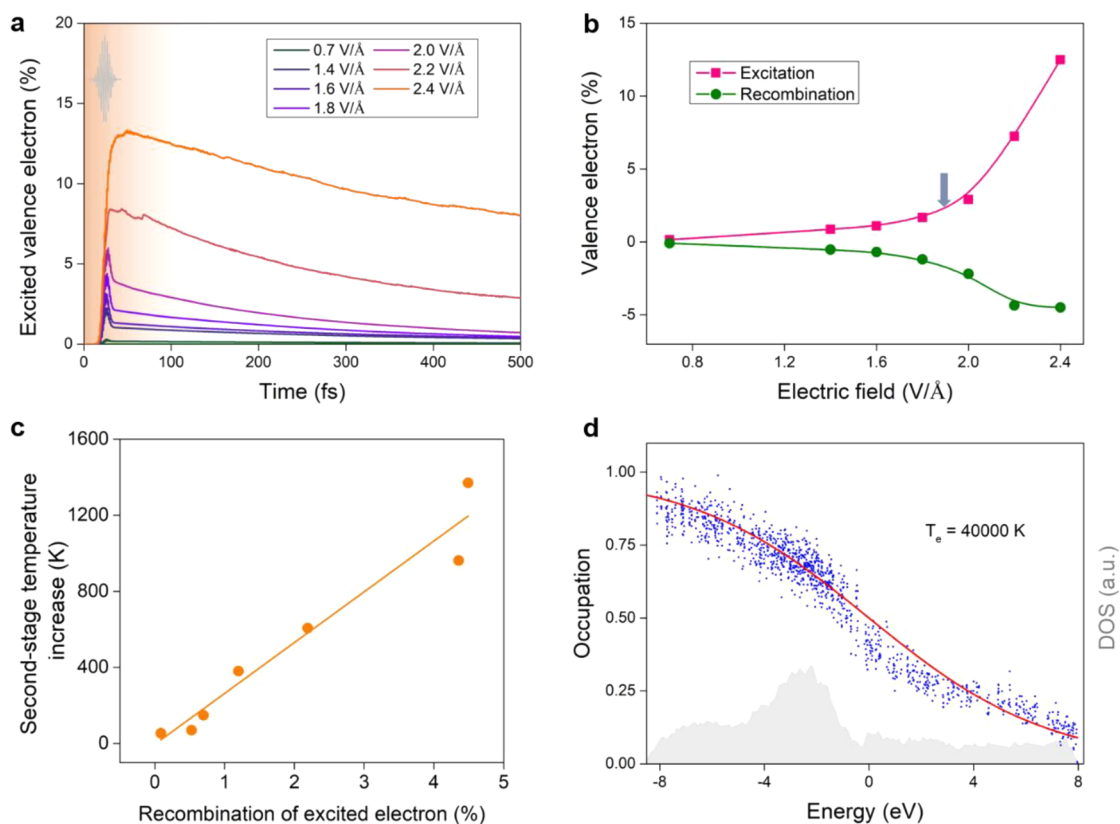


**Figure 4.** Electronic dynamics of liquid water. (a) Temporal evolutions of excited valence electrons with the electric field of laser pulses. (b) Effective electron excitation and electron recombination with electric fields of laser pulses. The arrow shows the transition from multiphoton to strong-field ionization processes. (c) Electron recombination vs the second-stage temperature increase of ionic subsystems. (d) Electronic occupation at  $t = 100$  fs in the simulation with an electric field of  $2.4$  V/Å. The instantaneous electronic density of states is also shown.

multiphoton to strong-field ionization processes (Figure 4b). The nonlinear electronic excitation directly leads to nonlinearity of first-stage (Figure S1c) and total (Figure S1b) pressure increases. Besides, nonlinear electronic excitation facilitates the field-induced stretch of OH bonds and the nonlinearity of first-stage ionic temperature increase (Figure 2b,c) and gives rise to the nonlinearity of second-stage ionic temperature increase via electronic recombination (Figure 4b,c).

**Plasma Generation.** Previous numerical simulations employ the criterion of the fraction of excited valence electrons of  $\sim 2\%$  for plasma generation in liquid water irradiated with picosecond and nanosecond laser pulses,<sup>5,41</sup> where the avalanche effects could enable the strong adsorptions of latter part of long pulses. However, with a single ultrashort laser pulse, the strong excitations of valence electrons are needed to drive the structural changes of ionic subsystems. With the laser pulse  $E_0 = 2.4$  V/Å, the severe structural changes are obtained (Figure 3c), and the instantaneous electronic temperature is  $\sim 40000$  K with  $\sim 12\%$  valence electrons excited at  $t = 100$  fs (Figure 4d). Moreover, the severe dissociation of water molecules introduces a metallic electronic density of states, confirming the emergence of water plasma (Figure 4d). Thus, the plasma generation is confirmed by both the fraction of excited valence electrons of  $\sim 12\%$  and the metallic electronic density of states. The threshold for plasma generations is  $2.4$  V/Å ( $\sim 7.6 \times 10^{13}$  W/cm<sup>2</sup>) for the ultrashort laser pulses used here, which is in the same order of  $\sim 2 \times 10^{13}$  W/cm<sup>2</sup> with the 10 fs long laser pulses.<sup>5</sup> The plasma state and violent

dissociated configuration emerge during the laser pulse of  $E_0 = 2.4$  V/Å ( $t - t_0 = \sim 11$  fs) (Figure S8) and remain within the 500 fs long simulation (Figure 3d). We note that the water plasma is the nonequilibrium state of liquid water following the intense photoexcitation, which has a density of  $1$  g/cm<sup>3</sup> and two nonequilibrium temperatures for the electronic ( $\sim 10^4$  K) and ionic ( $\sim 10^3$  K) subsystem, respectively. Similar plasma generation processes were detected with the ultrafast X-ray irradiation, where X-ray-induced plasma emerges within the first 5 fs of the pulses and has the ionic temperature of  $\sim 10^4$  K and the system pressure of  $\sim 10^3$  kbar due to severe electronic excitations.<sup>14</sup> The broadened distribution of oxygen–oxygen RDF of water plasma found in the present work is consistent with that of X-ray-induced water plasma (inset of Figure 2d), but our *ab initio* simulations reveal the formation of a large amount of free protons ( $\sim 50\%$ ) and various transient species in nonequilibrium water plasma. The plasma generation is coincident with the slowdown of electron recombination rate (Figure 4b and Figure S9), reflecting that the formation of intermediate species stabilizes the electronic excited state and delays the recombination of charge carriers.

## CONCLUSION

Our nonadiabatic *ab initio* molecular dynamics simulations reveal the initial ionic and electronic dynamics and energy transfer pathways of photoexcited liquid water. We found that water undergoes a two-step heating and pressurization process upon photoexcitation. The strong-field effects of laser pulses and the electron excitations contribute to the first-stage heating

and pressurization. The subsequent electron–ion interactions lead to energy transfer from the electronic subsystem to the ionic subsystem, and liquid water then undergoes the second-stage heating. Recombination of excited valence electron releases the great internal pressure during the relaxation processes. The laser pulses greatly stretch water molecules during laser irradiation, and the electronic excitations lead to proton transfers after laser pulses. The intense laser pulses drastically excite liquid water, giving rise to severe water dissociation and the generation of water plasma. The nonequilibrium water plasma exhibits the separate ionic and electronic temperatures, metallic electronic density of states, and highly dissociated configurations. The study of photoexcited dynamics not only offers a fundamental understanding of ultrafast processes and nonequilibrium states of liquid water but also provides new insights into the possible modulations of light–matter interactions. What is more, the exploration of photoexcited dynamics in water will benefit the microscopic understanding of photochemical reactions<sup>42</sup> and photoinduced phase transitions.<sup>43,44</sup> Besides, the nonequilibrium water plasma may enable the ultrafast and efficient laser-based catalyzing, synthesis, and manufacturing in aqueous medium.

## METHODS

### Nonadiabatic *Ab Initio* Molecular Dynamics Simulations.

The nonadiabatic *ab initio* molecular dynamics simulations were performed via the recent implementations of rt-TDDFT algorithms<sup>45</sup> in Quantum Espresso.<sup>46</sup> The optimized norm-conserving Vanderbilt (ONCV) pseudopotentials<sup>47</sup> and the energy cutoff of 85 Ry were used in all the simulations. We chose the van der Waals density functional using the optB88-vdW method<sup>48</sup> to account for the hydrogen-bond networks of liquid water. Liquid water was modeled by using a periodic 32-water-molecule cubic supercell with the density of 1 g/cm<sup>3</sup>. The Brillouin zone was sampled with a  $2 \times 2 \times 2$  k-point mesh to describe well the unoccupied electronic density of states of liquid water,<sup>49</sup> and 52 unoccupied electronic states were considered in the nonadiabatic simulations. The calculated band gap of  $\sim 4.1$  eV is less than the experimental one of 8.7 eV, while it is consistent with the GGA results of 4.36 eV.<sup>50</sup> The time step of nuclei is 0.0484 fs, and the time step of electrons is 0.0968 as. The accuracy enables the nonadiabatic *ab initio* simulations of 500 fs (Figure S10), and this time scale is long enough to track the initial ionic and electronic dynamics of liquid water upon photoexcitation.

**Laser Pulse Parameters.** The liquid water was first equilibrated for 12 ps at 300 K in NVT ensemble. Then, the obtained configuration of liquid water was isochorically irradiated with the laser pulse of  $E(t) = E_0 \cos[2\pi(c/\lambda)t] \exp[-(t - t_0)^2/2\sigma^2]$ . We used the pulses with the wavelength  $\lambda = 800$  nm and the width  $\sigma = 5$  fs centered at  $t_0 = 24$  fs. The electric field  $E_0$  of laser pulses ranges from 0.7 to 2.4 V/Å, and the corresponding peak intensities are on the order of  $10^{13}$  W/cm<sup>2</sup>. The photon energy of 1.55 eV is less than both the theoretical and experimental band gaps of liquid water. The velocity gauge is used to enable the periodic electric fields in nonadiabatic simulations.<sup>51</sup> The ultrafast pulses enable the separation and detection of the successive dynamics of photoexcited liquid water.<sup>12</sup>

## ASSOCIATED CONTENT

### Supporting Information

The Supporting Information is available free of charge at <https://pubs.acs.org/doi/10.1021/jacs.1c04675>.

Additional information about pressure evolution, energy absorption, structural evolution, and electronic evolution of photoexcited liquid water (PDF)

## AUTHOR INFORMATION

### Corresponding Author

**Sheng Meng** – Beijing National Laboratory for Condensed Matter Physics and Institute of Physics, Chinese Academy of Sciences, Beijing 100190, People's Republic of China; School of Physical Sciences, University of Chinese Academy of Sciences, Beijing 100049, People's Republic of China; Songshan Lake Materials Laboratory, Dongguan, Guangdong 523808, People's Republic of China; [orcid.org/0000-0002-1553-1432](https://orcid.org/0000-0002-1553-1432); Email: [smeng@iphy.ac.cn](mailto:smeng@iphy.ac.cn)

### Authors

**Jiyu Xu** – Beijing National Laboratory for Condensed Matter Physics and Institute of Physics, Chinese Academy of Sciences, Beijing 100190, People's Republic of China; [orcid.org/0000-0002-2628-5492](https://orcid.org/0000-0002-2628-5492)

**Daqiang Chen** – Beijing National Laboratory for Condensed Matter Physics and Institute of Physics, Chinese Academy of Sciences, Beijing 100190, People's Republic of China; School of Physical Sciences, University of Chinese Academy of Sciences, Beijing 100049, People's Republic of China

Complete contact information is available at:

<https://pubs.acs.org/10.1021/jacs.1c04675>

### Notes

The authors declare no competing financial interest.

## ACKNOWLEDGMENTS

We acknowledge financial support from the National Natural Science Foundation of China (No. 12025407, 11934003, 91850120, and 11774396), National Key Research and Development Program of China (No. 2016YFA0300902), and “Strategic Priority Research Program (B)” of Chinese Academy of Sciences (Grant XDB330301).

## REFERENCES

- (1) Garrett, B. C.; et al. Role of water in electron-initiated processes and radical chemistry: Issues and scientific advances. *Chem. Rev.* **2005**, *105*, 355–390.
- (2) Fujishima, A.; Honda, K. Electrochemical photolysis of water at a semiconductor electrode. *Nature* **1972**, *238*, 37–38.
- (3) Wang, X.; et al. A metal-free polymeric photocatalyst for hydrogen production from water under visible light. *Nat. Mater.* **2009**, *8*, 76–80.
- (4) Klán, P.; Holoubek, I. Ice (photo)chemistry.: Ice as a medium for long-term (photo)chemical transformations—environmental implications. *Chemosphere* **2002**, *46*, 1201–1210.
- (5) Vogel, A.; Noack, J.; Hüttman, G.; Paltauf, G. Mechanisms of femtosecond laser nanosurgery of cells and tissues. *Appl. Phys. B: Lasers Opt.* **2005**, *81*, 1015–1047.
- (6) Hart, E. J.; Boag, J. W. Absorption spectrum of the hydrated electron in water and in aqueous solutions. *J. Am. Chem. Soc.* **1962**, *84*, 4090–4095.
- (7) Elkins, M. H.; Williams, H. L.; Shreve, A. T.; Neumark, D. M. Relaxation mechanism of the hydrated electron. *Science* **2013**, *342*, 1496.
- (8) Li, J.; Nie, Z.; Zheng, Y. Y.; Dong, S.; Loh, Z.-H. Elementary electron and ion dynamics in ionized liquid water. *J. Phys. Chem. Lett.* **2013**, *4*, 3698–3703.
- (9) Loh, Z. H.; et al. Observation of the fastest chemical processes in the radiolysis of water. *Science* **2020**, *367*, 179.
- (10) Strycker, B. D.; et al. Femtosecond-laser-induced shockwaves in water generated at an air-water interface. *Opt. Express* **2013**, *21*, 23772–23784.

- (11) Schaffer, C. B.; Nishimura, N.; Glezer, E. N.; Kim, A. M. T.; Mazur, E. Dynamics of femtosecond laser-induced breakdown in water from femtoseconds to microseconds. *Opt. Express* **2002**, *10*, 196–203.
- (12) Rethfeld, B.; Ivanov, D. S.; Garcia, M. E.; Anisimov, S. I. Modelling ultrafast laser ablation. *J. Phys. D: Appl. Phys.* **2017**, *50*, 193001.
- (13) Sundaram, S. K.; Mazur, E. Inducing and probing non-thermal transitions in semiconductors using femtosecond laser pulses. *Nat. Mater.* **2002**, *1*, 217–224.
- (14) Beyerlein, K. R.; et al. Ultrafast nonthermal heating of water initiated by an X-ray Free-Electron Laser. *Proc. Natl. Acad. Sci. U. S. A.* **2018**, *115*, 5652.
- (15) Klein, A. L.; et al. Drop shaping by laser-pulse impact. *Phys. Rev. Appl.* **2015**, *3*, 044018.
- (16) Vogel, A.; Linz, N.; Freidank, S.; Paltauf, G. Femtosecond-laser-induced nanocavitation in water: Implications for optical breakdown threshold and cell surgery. *Phys. Rev. Lett.* **2008**, *100*, 038102.
- (17) Stan, C. A.; et al. Negative pressures and spallation in water drops subjected to nanosecond shock waves. *J. Phys. Chem. Lett.* **2016**, *7*, 2055–2062.
- (18) Stan, C. A.; et al. Liquid explosions induced by X-ray laser pulses. *Nat. Phys.* **2016**, *12*, 966–971.
- (19) Courvoisier, F.; Boutou, V.; Favre, C.; Hill, S. C.; Wolf, J.-P. Plasma formation dynamics within a water microdroplet on femtosecond time scales. *Opt. Lett.* **2003**, *28*, 206–208.
- (20) Lindinger, A.; et al. Time-resolved explosion dynamics of H<sub>2</sub>O droplets induced by femtosecond laser pulses. *Appl. Opt.* **2004**, *43*, 5263–5269.
- (21) Thürmer, S.; et al. On the nature and origin of dicationic, charge-separated species formed in liquid water on X-ray irradiation. *Nat. Chem.* **2013**, *5*, 590–596.
- (22) Marsalek, O.; et al. Chasing charge localization and chemical reactivity following photoionization in liquid water. *J. Chem. Phys.* **2011**, *135*, 224510.
- (23) Mishra, P. K.; Vendrell, O.; Santra, R. Ultrafast energy transfer to liquid water by sub-picosecond high-intensity terahertz pulses: An abinitio molecular dynamics study. *Angew. Chem., Int. Ed.* **2013**, *52*, 13685–13687.
- (24) Andersson, S.; Al-Halabi, A.; Kroes, G.-J.; van Dishoeck, E. F. Molecular-dynamics study of photodissociation of water in crystalline and amorphous ices. *J. Chem. Phys.* **2006**, *124*, 064715.
- (25) Andersson, S.; Kroes, G.-J.; van Dishoeck, E. F. Photodissociation of water in crystalline ice: A molecular dynamics study. *Chem. Phys. Lett.* **2005**, *408*, 415–421.
- (26) Crouse, J.; Loock, H. P.; Cann, N. M. The photoexcitation of crystalline ice and amorphous solid water: A molecular dynamics study of outcomes at 11 and 125 K. *J. Chem. Phys.* **2015**, *143*, 034502.
- (27) Yan, L.; Xu, J.; Wang, F.; Meng, S. Plasmon-induced ultrafast hydrogen production in liquid water. *J. Phys. Chem. Lett.* **2018**, *9*, 63–69.
- (28) Miyamoto, Y.; Zhang, H.; Cheng, X.; Rubio, A. Modeling of laser-pulse induced water decomposition on two-dimensional materials by simulations based on time-dependent density functional theory. *Phys. Rev. B: Condens. Matter Mater. Phys.* **2017**, *96*, 115451.
- (29) Miyamoto, Y.; Zhang, H.; Cheng, X.; Rubio, A. Ab initio simulation of laser-induced water decomposition close to carbon nanotubes. *Phys. Rev. B: Condens. Matter Mater. Phys.* **2019**, *99*, 165424.
- (30) Kumar, A.; Kolaski, M.; Lee, H. M.; Kim, K. S. Photoexcitation and photoionization dynamics of water photolysis. *J. Phys. Chem. A* **2008**, *112*, 5502–5508.
- (31) Wang, Z. P.; Dinh, P. M.; Reinhard, P. G.; Suraud, E. Ultrafast nonadiabatic dynamics of a water dimer in femtosecond laser pulses. *Laser Phys.* **2014**, *24*, 106004.
- (32) Stetina, T. F.; Sun, S.; Lingerfelt, D. B.; Clark, A.; Li, X. The role of excited-state proton relays in the photochemical dynamics of water nanodroplets. *J. Phys. Chem. Lett.* **2019**, *10*, 3694–3698.
- (33) Lu, L.; et al. The “hole” story in ionized water from the perspective of ehrenfest dynamics. *J. Phys. Chem. Lett.* **2020**, *11*, 9946–9951.
- (34) Saitta, A. M.; Saija, F.; Giaquinta, P. V. Ab initio molecular dynamics study of dissociation of water under an electric field. *Phys. Rev. Lett.* **2012**, *108*, 207801.
- (35) Chin, S. L.; Lagacé, S. Generation of H<sub>2</sub>, O<sub>2</sub>, and H<sub>2</sub>O<sub>2</sub> from water by the use of intense femtosecond laser pulses and the possibility of laser sterilization. *Appl. Opt.* **1996**, *35*, 907–911.
- (36) Kaiser, A.; Rethfeld, B.; Vicanek, M.; Simon, G. Microscopic processes in dielectrics under irradiation by subpicosecond laser pulses. *Phys. Rev. B: Condens. Matter Mater. Phys.* **2000**, *61*, 11437–11450.
- (37) Keldysh, L. Ionization in the field of a strong electromagnetic wave. *Sov. Phys. JETP* **1965**, *20*, 1307–1314.
- (38) Ma, Q.; et al. Extremely low electron-ion temperature relaxation rates in warm dense hydrogen: Interplay between quantum electrons and coupled ions. *Phys. Rev. Lett.* **2019**, *122*, 015001.
- (39) Elles, C. G.; Jailaubekov, A. E.; Crowell, R. A.; Bradforth, S. E. Excitation-energy dependence of the mechanism for two-photon ionization of liquid H<sub>2</sub>O and D<sub>2</sub>O from 8.3 to 12.4 eV. *J. Chem. Phys.* **2006**, *125*, 044515.
- (40) Savolainen, J.; Uhlig, F.; Ahmed, S.; Hamm, P.; Jungwirth, P. Direct observation of the collapse of the delocalized excess electron in water. *Nat. Chem.* **2014**, *6*, 697–701.
- (41) Favre, C.; et al. White-light nanosource with directional emission. *Phys. Rev. Lett.* **2002**, *89*, 035002.
- (42) Martín, F.; et al. Single photon-induced symmetry breaking of H<sub>2</sub> dissociation. *Science* **2007**, *315*, 629–633.
- (43) Chakarov, D.; Kasemo, B. Photoinduced crystallization of amorphous ice films on graphite. *Phys. Rev. Lett.* **1998**, *81*, 5181–5184.
- (44) Bergsman, D. S.; Getachew, B. A.; Cooper, C. B.; Grossman, J. C. Preserving nanoscale features in polymers during laser induced graphene formation using sequential infiltration synthesis. *Nat. Commun.* **2020**, *11*, 3636.
- (45) Lian, C.; Zhang, S.-J.; Hu, S.-Q.; Guan, M.-X.; Meng, S. Ultrafast charge ordering by self-amplified exciton–phonon dynamics in TiSe<sub>2</sub>. *Nat. Commun.* **2020**, *11*, 43.
- (46) Giannozzi, P.; et al. QUANTUM ESPRESSO: a modular and open-source software project for quantum simulations of materials. *J. Phys.: Condens. Matter* **2009**, *21*, 395502.
- (47) Hamann, D. R. Optimized norm-conserving Vanderbilt pseudopotentials. *Phys. Rev. B: Condens. Matter Mater. Phys.* **2013**, *88*, 085117.
- (48) Klimeš, J.; Bowler, D. R.; Michaelides, A. Chemical accuracy for the van der Waals density functional. *J. Phys.: Condens. Matter* **2010**, *22*, 022201.
- (49) Prendergast, D.; Grossman, J. C.; Galli, G. The electronic structure of liquid water within density-functional theory. *J. Chem. Phys.* **2005**, *123*, 014501.
- (50) Chen, W.; Ambrosio, F.; Miceli, G.; Pasquarello, A. Ab initio electronic structure of liquid water. *Phys. Rev. Lett.* **2016**, *117*, 186401.
- (51) Guan, M.-X.; et al. Cooperative evolution of intraband and interband excitations for high-harmonic generation in strained MoS<sub>2</sub>. *Phys. Rev. B: Condens. Matter Mater. Phys.* **2019**, *99*, 184306.